Journal of Biomechanics 147 (2023) 111458

Contents lists available at ScienceDirect

Journal of Biomechanics

journal homepage: www.elsevier.com/locate/jbiomech

Short communication

In vitro bioreactor for mechanical control and characterization of tissue constructs

Samuel J. Coeyman [a], Yuhua Zhang [b], Catalin F. Baicu [b,c], Michael R. Zile [b,c], Amy D. Bradshaw [b,c], William J. Richardson [d,*]

[a] Department of Bioengineering, Clemson University, Clemson, SC, USA
[b] Gazes Cardiac Research Institute, Division of Cardiology, Department of Medicine, Medical University of South Carolina, USA
[c] Ralph H. Johnson Department of Veterans Affairs Medical Center, Charleston, SC, USA
[d] Department of Chemical Engineering, University of Arkansas, Fayetteville, AR, USA

ARTICLE INFO

Keywords:
Fibroblast
Fibrin gel
In vitro platform
Bioreactor
Mechanical analysis
Tissue engineering
Fibrosis
Heart failure

ABSTRACT

Cardiac fibrosis is a key contributor to the onset and progression of heart failure and occurs from extracellular matrix accumulation via activated cardiac fibroblasts. Cardiac fibroblasts activate in response to mechanical stress and have been studied in the past by applying forces and deformations to three-dimensional, cell-seeded gels and tissue constructs in vitro. Unfortunately, previous stretching platforms have traditionally not enabled mechanical property assessment to be performed with an efficient throughput, thereby limiting the full potential of in vitro mechanobiology studies. We have developed a novel in vitro platform to study cell-populated tissue constructs under dynamic mechanical stimulation while also performing repeatable, non-destructive stress–strain tests in living constructs. Additionally, this platform can perform these tests across all constructs in a multi-well plate simultaneously, providing exciting potential for direct, functional readouts in future screening applications. In our pilot application, we showed that cyclically stretching cell-populated tissue constructs composed of murine cardiac fibroblasts within a 3D fibrin matrix leads to collagen accumulation and increased tissue stiffness over a three-day time course. Results of this study validate our platform's ability to apply mechanical loads to tissues while performing live mechanical analyses to observe cell-mediated tissue remodeling.

1. Introduction

The important role of mechanical stimulation in a wide range of disease conditions has led many groups to investigate cell behavior in controlled mechanical contexts in vitro (Hackett et al., 2022; Hou et al., 2017; Kural and Billiar, 2016; Miyazaki et al., 2019; Parsa et al., 2017; Rogers et al., 2021; Schmidt et al., 2016; Walker et al., 2020a–c; Zhang et al., 2019; Smithmyer et al., 2014). However, a major limitation of most current platforms is that mechanical property analysis of a cell-populated tissue construct (hereafter referred to simply as "tissue") cannot be performed in a multi-well fashion, limiting the throughput potential of in vitro screens. In this study, we developed a multi-well in vitro tissue culture platform capable of performing stress–strain tests across numerous cell-seeded gels at the same time. As an initial demonstration, we used our platform to test the hypothesis that cyclically stretching cardiac fibroblasts within a 3D fibrin matrix would lead to collagen accumulation and increased tissue modulus.

2. Materials and methods

2.1. Platform design

Custom six-well plates (Fig. 1A) were 3D-printed out of Dental LT resin (FormLabs RS-F2-DLCL-02) with a Form 2 printer (FormLabs PKG-F2). Within each well was a set of grips on a 3D printed piston embedded with a cubed magnet (SuperMagnetMan C0010), and a set of grips attached to the wall opposite of the piston. The magnetic piston is attracted to an external electromagnet (McMaster 5684 K23), whose properties are customized through a computer-controlled DC power supply (Siglent SPD3303X-E). Using this setup provides the capability to apply an attractive force between 0 and 7.5 mN for stretching tissues to a max strain of 40% at a strain rate between 0 and 0.55 Hz. Full design details and power-supply control codes are available at https://github.com/SysMechBioLab/BioreactorControls.

* Corresponding author at: 3149 Bell Engineering Center, 800 West Dickson St, Fayetteville, AR 72701, USA.
E-mail address: wr013@uark.edu (W.J. Richardson).

https://doi.org/10.1016/j.jbiomech.2023.111458
Accepted 13 January 2023
Available online 18 January 2023

2.2. Tissue fabrication

On the day of making gels, a spacer (Fig. 1B.1) was inserted between each piston and the well wall to provide space for stretching after tissue formation. The well plate - piston - spacer combination was then placed flush against a permanent strip magnet (SuperMagnetMan Rect5050) orientated so the permanent magnet attracts the magnetic pistons (Fig. 1B). The entire setup was disinfected, each well was washed with Pluronic F-127 to limit tissue adhesion, and 90 uL of fibrin gel mixture was poured into each well. Fibrin gel mixture consisted of primary cardiac fibroblasts harvested from male and female C57/B16 mice (n = 9 different biological replicates) at 12–16 weeks of age, resuspended at 420,000 cells per mL in a 1:1 solution containing 0.44 U/mL bovine thrombin (Sigma T4648-1KU) and 6.6 mg/mL fibrinogen (Fisher 50–176-5054). Tissues were incubated at 37 °C for 1 h to allow for initial formation, covered with DMEM containing 5% FBS, 20 ug/mL L-ascorbic acid (Sigma A92902) and 10 ng/mL TGFβ (R&D Systems 240-B), and incubated overnight at 37 °C (Fig. 1C).

The next day, media was exchanged with DMEM containing 5% FBS and 20 ug/mL ascorbic acid and the well plate was separated from the strip magnet with spacers removed (Fig. 1B). A stress–strain test was performed (described in 2.3), and tissues were left to uniaxially stretch cyclically in the incubator at an average of ~10% stretch and 0.27 Hz (chosen because of power supply response time). For each of the next 3 days, a media change containing ascorbic acid was performed, a stress–strain test was conducted, and cyclic stretching was continued.

2.3. Mechanical testing

Uniaxial stress–strain tests were conducted by stepwise increasing an attractive force from the electromagnet to the magnetic pistons using a custom LabVIEW program to control the DC power supply and a microscope camera for video-capture (Fig. 1D, code available at https://github.com/SysMechBioLab/BioreactorControls). Stress–strain videos were analyzed using a custom code in MATLAB, which automatically tracked the centroid coordinates of each magnetic piston to determine bulk displacements of the construct (Fig. 2A, codes available at https://github.com/SysMechBioLab/BioreactorControls). Using the camera with MATLAB allows for repeatable strain measurements for 1920x1080 pixel, 60 frame per second videos on a frame-by-frame basis with measuring resolutions of ~45 um/pixel.

Stresses experienced by the tissues were calculated by dividing the electromagnet's attractive force by the tissue's cross-sectional area. Forces were calibrated by measuring magnet-induced compression of polyurethane standards matched to identical compression under known weights. Briefly, 3x1.5x1.5 mm polyurethane foam blocks were placed behind magnetic pistons to be sandwiched under ramping currents (0–0.7A). Images of the blocks before and after compression were processed in ImageJ to calculate how much strain occurred at each current. Next, the polyurethane blocks were placed within a custom weight drop rig to be compressed under known weights. Pictures of block compression were taken and processed in ImageJ to determine the strain experienced under known weights, which was then used as a calibration curve for calculating how much force was applied by the electromagnet on the magnetic piston at each current setting. A detailed description of this process is available at https://github.com/SysMechBioLab/BioreactorControls.

Tissue compaction was measured as the tissue minimum width divided by the initial tissue width, and cross-sectional area was calculated by taking the minimum width measurement and multiplying it by tissue thickness, which was estimated by multiplying tissue compaction times initial tissue thickness. Young's moduli (kPa) were determined by plotting stresses vs strains for each tissue. For our tissues, these stress–strain plots exhibited linear relationships, so the slope of the best-fit-line was taken as the modulus for each tissue (Fig. 1E). Linear relationships between electromagnet attractive force and displacement were also used to determine linear stiffness (mN/mm) through best fit lines of total force vs. bulk displacement plots. Compaction, modulus, and linear stiffness data for each tissue were recorded and each compared through three statistical tests: paired *t*-test between day 0 and day 3 values for non-stretched tissues, paired *t*-test between day 0 and day 3 values for stretched tissues, and unpaired *t*-test between day 3 values for non-stretched and stretched tissues. A Bonferroni adjustment was applied to p-values from each statistical test in order to correct for multi-comparisons (n = 3) within the study.

2.4. Immunofluorescent analysis

Tissues were collected at the end of the 3-day stretch period to perform immunofluorescence microscopy analysis. Collecting the tissues consisted of removing the media from each well and fixing with 4% paraformaldehyde (Sigma 158127). Staining of the tissues consisted of a

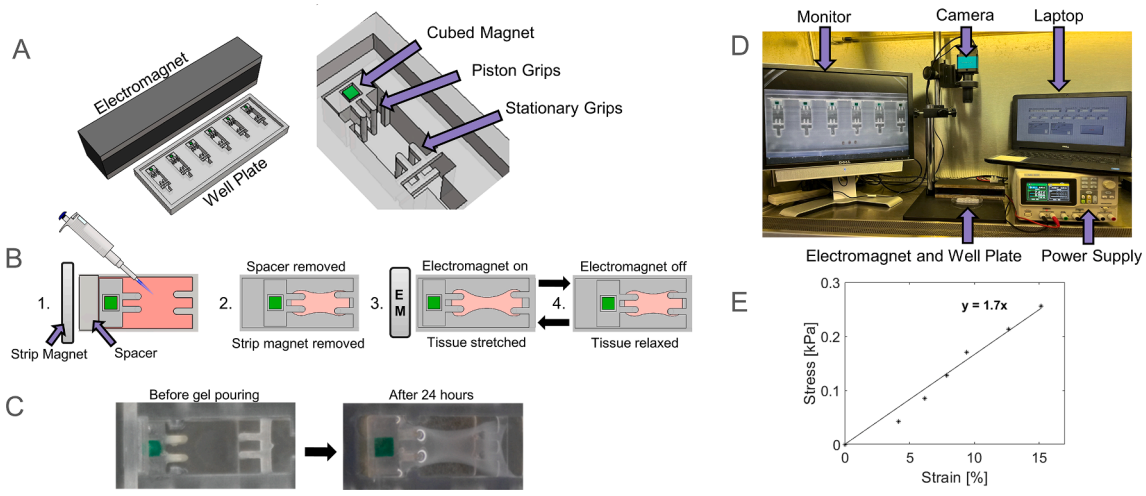

Fig. 1. In Vitro Platform Design. Within the custom 3D-printed multiwell plates, each rectangular well included stationary grips affixed to the wall of one end of the well, and another set of grips affixed on the opposite end to a movable piston component (A, B). The piston was embedded with a permanent magnet, allowing an external, computer-controlled electromagnet to uniaxially pull the piston with calibrated forces. Cell-seeded fibrin tissues were polymerized within the wells (B, C) such that each tissue was held onto the opposing sets of grips. Imaging the full plate during force-controlled extension tests (D) enabled image-based displacement measurements to produce repetitive, non-destructive stress–strain characterizations of all the tissues simultaneously (E).

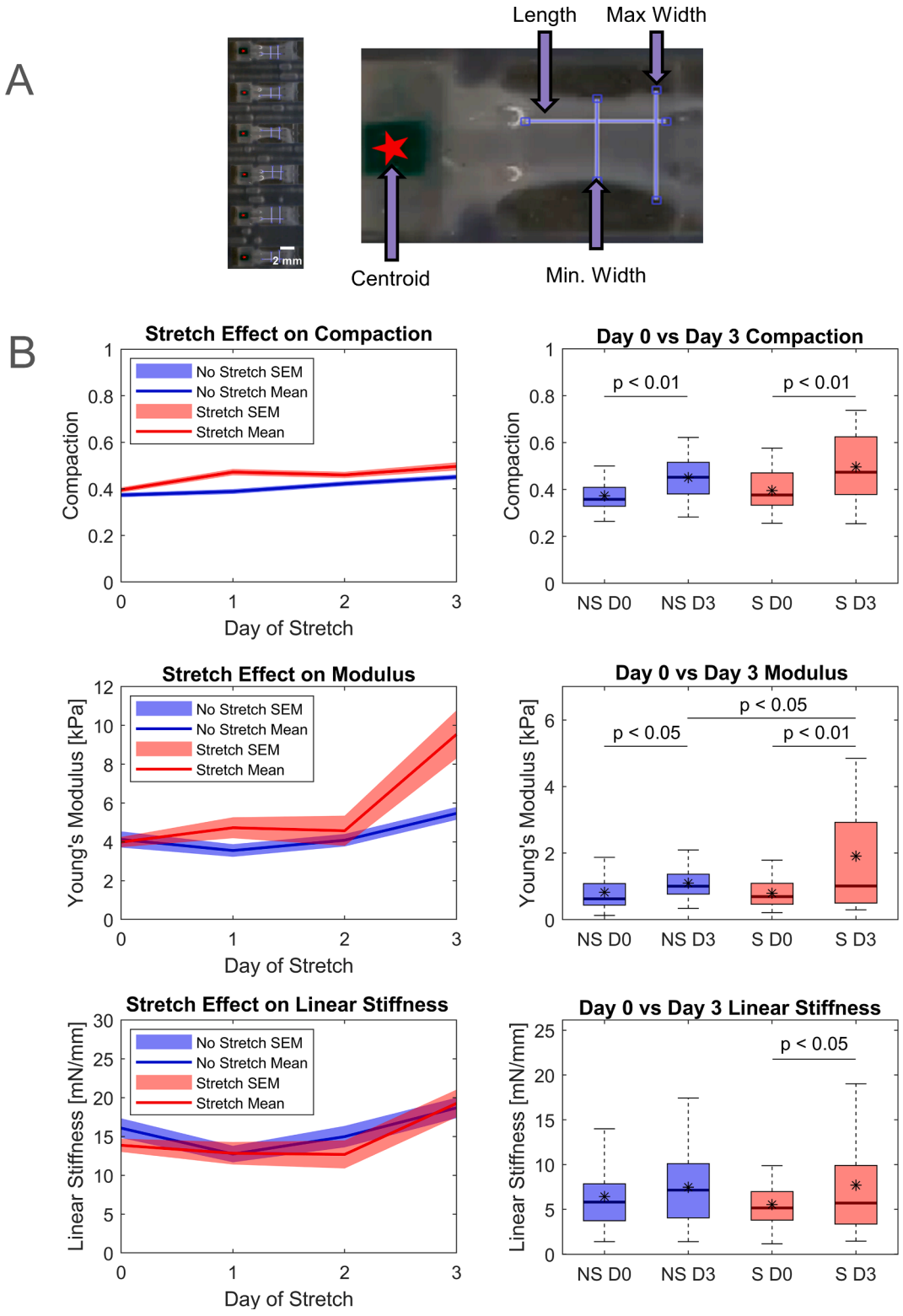

Fig. 2. Mechanical Characterization of Tissue Constructs. Each cell-seeded tissue across the 6-well plate underwent daily stress–strain tests by video-tracking piston displacements during magnet-induced uniaxial deformation. Both unstretched and stretched tissue groups showed slight compaction from day 0 to day 3 as well as increased Young's moduli, but stretched tissues showed much larger increases in Young's moduli than unstretched tissues. Stretched tissues showed increased linear stiffness values from day 0 to day 3, but these did not show statistical differences with the unstretched tissues.

PBS wash, blocking, and adding primary antibody solution consisting of collagen IV (Novus NB110-59981) and phalloidin conjugated to 545 (Sigma P1951). Phalloidin was chosen to stain the fibroblast F-actin cytoskeleton and collagen IV was selected as a protein of interest because it is an important component of both healthy and diseased hearts (Bruggink et al. (2007), Chapman et al. (1990) Oct). Images of stained tissues were taken on a benchtop confocal microscope through a 20X objective lens on an Olympus 102 BX53 upright microscope.

Images from 3 random regions within each tissue were loaded into a CellProfiler pipeline to be processed for cell number, cell morphology, and collagen intensity. For each image, the pipeline utilized the blue (DAPI) channel to find cell nuclei, count the nuclei to get cell number, and then store the nuclei as objects. The nuclei objects were then used as center points for watershed propagation with the red (TRITC) channel to trace each cell's F-actin cytoskeleton and provide cell body outlines.

Cell outlines were utilized to calculate cell area and cell eccentricity, calculated as the ratio of the distance between the foci of an ellipse fitted to the cell outline and that ellipse's major axis length. A higher value in eccentricity means the ellipse is more elongated where a value of 0 is a perfect circle (Carpenter et al., 2006). Cell orientations were used to calculate bulk cell alignment, calculated as a mean vector length (MVL) using Equation (1) (Richardson et al., 2015; Richardson and Holmes, 2016).

$$MVL = \sqrt{\left(\frac{\Sigma cos(2\alpha)}{n}\right)^2 + \left(\frac{\Sigma sin(2\alpha)}{n}\right)^2} \quad (1)$$

Equation (1) utilizes orientation angles (α) from the cell outlines in the tissues and the total number of cells used in the set (n) to calculate an alignment value for the entire tissue, where 0 is random and a value is 1 is perfectly aligned.

Collagen IV levels were assessed by quantifying the total green (488) intensity signal in each image and then normalized by cell counts for each image to obtain a collagen amount per cell. Each immunohistochemistry output was processed through a two-sample *t*-test in MATLAB to perform statistical analyses between the stretched and unstretched groups.

3. Results

3.1. Mechanical data

A total of 58 stretch tissues and 51 unstretched tissues (~13 tissues per mouse) were subjected to stress–strain tests. Both unstretched and stretched tissue groups compacted from day 0 to day 3 ($p < 0.01$), but no significant differences in compaction between the unstretched and stretched groups (Fig. 2A-B). Results from the mechanical tests showed that stretching of the fibroblasts led to a stiffer tissue across the three day stretch period (Fig. 2B). Although both stretch and no stretch groups did get stiffer over time, the stretch group stiffened more dramatically with day 3 Young's moduli significantly greater than unstretched tissues' day 3 moduli ($p < 0.01$). Stretched tissues also showed increases in linear stiffness values from day 0 to day 3, but these did not show statistical differences with the unstretched tissues.

3.2. Morphology and collagen data

Stained images from 31 stretched tissues and 27 unstretched tissues were imported into the CellProfiler pipeline to find cell nuclei and cell outlines for counts and morphology measurements (Fig. 3). Counting the number of cells determined that the stretch and no stretch groups had similar cell counts ($p > 0.95$). Cell outlines revealed that the stretching led to larger cells ($p < 0.01$) that were more elongated ($p < 0.01$) and more aligned ($p < 0.01$) than cells in non-stretched tissues.

Staining for collagen IV in stretched and unstretched tissues revealed that collagen was produced in both conditions, detected within cells and also in extracellular compartments represented in a sheet-like form (Fig. 3B). Quantifying collagen intensity found that stretching led to increased Col IV immunoreactivity levels in stretched versus unstretched tissues ($p < 0.01$, Fig. 3C).

4. Discussion

Various fibrosis-specific treatments with promising results in pre-clinical studies have been unsuccessful in demonstrating clinical therapeutic benefit (Ichihara et al., 2002; Frantz et al., 2008; Ma et al., 2013; Hammoud et al., 2011). In vitro platforms offer capabilities to screen large sets of compounds prior to animal studies, but there is an important need for these in vitro platforms to be able to subject cells to variable mechanical stimulation akin to the in vivo context of a beating heart (Richardson et al., 2021). Further, there is a need for platforms to also enable assessment of the mechanical properties of in vitro tissues in order to assess the effects of biological perturbations and drug candidates on a primary functional readout related to HF, e.g., tissue stiffness. Our novel platform enabled dynamic mechanical characterization of cell-mediated tissue remodeling in vitro - a capability not possible in standard 3D tissue culture. As hypothesized, cyclic stretching led to greater cell elongation, cell alignment, collagen production, and increased tissue modulus in comparison to unstretched tissues. This multi-well platform offers potential as a screening tool for assessing the effect of different treatments on clinically relevant metrics of tissue stiffness using automated measurements. Though not performed herein, the platform also allows for measurements of cell-generated forces during acute contraction (e.g., myocyte twitches) or chronic tissue compaction. Future studies with this platform enable tests of

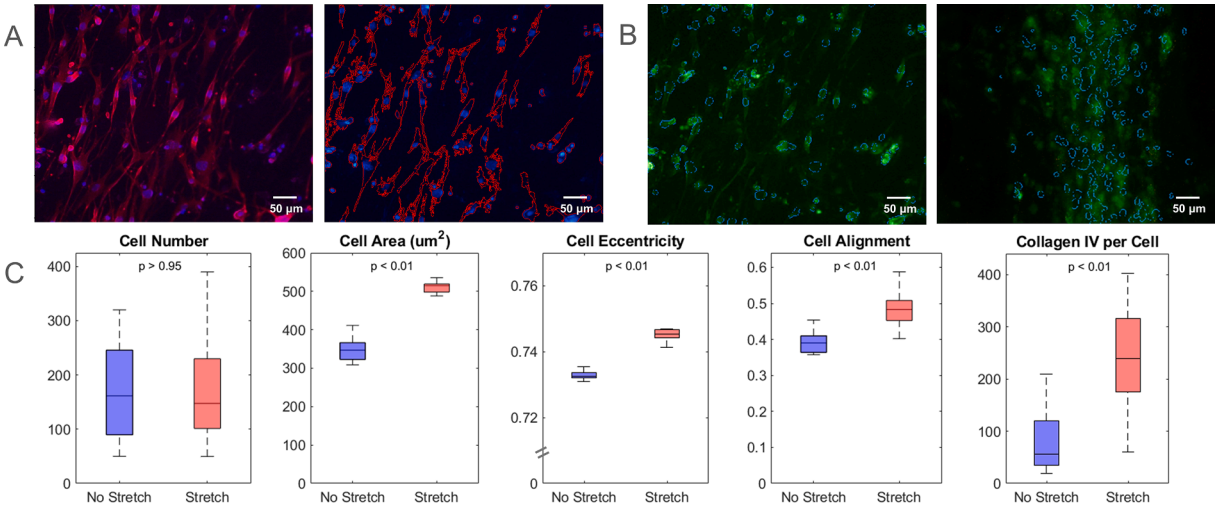

Fig. 3. Effect of Stretching on Cell Morphology and Collagen Accumulation. Immunofluorescent microscopy and quantitative image processing were used to quantify cell morphology and collagen levels after 3 days of culture. Tissues subjected to dynamic stretching for 3 days showed similar levels of cell density but greater cell area, cell eccentricity, cell alignment, and collagen IV intensity levels compared to non-stretched tissues.

fundamental mechanobiology hypotheses relating to force vs. displacement control of cells, mechanical homeostasis in remodeling tissues, and dynamic cell-matrix feedback loops.

CRediT authorship contribution statement

Samuel J. Coeyman: Writing - original draft, Writing - review & editing, Visualization, Validation, Software, Methodology, Investigation, Forma analysis, Data curation, Conceptualization. **Yuhua Zhang:** Investigation, Methodology, Writing - review & editing. **Catalin F. Baicu:** Supervision, Methodology, Writing - review & editing. **Michael R. Zile:** Conceptualization, Writing - review & editing. **Amy D. Bradshaw:** Supervision, Resources, Methodology, Funding acquisition, Conceptualization, Writing - review & editing. **William J. Richardson:** Visualization, Supervision, Resources, Project administration, Funding acquisition, Formal analysis, Conceptualization, Writing - review & editing.

Declaration of Competing Interest

The authors declare that they have no known competing financial interests or personal relationships that could have appeared to influence the work reported in this paper.

Acknowledgements

We would like to acknowledge support to complete this research from the American Heart Association [17SDG33410658], National Institutes of Health [GM121342, HL144927], SC EPSCoR [21-GE04], and the Veterans Administration [CX001608].

References

Bruggink, A.H., van Oosterhout, M.F.M., de Jonge, N., Cleutjens, J.P.M., van Wichen, D. F., van Kuik, J., Tilanus, M.G.J., Gmelig-Meyling, F.H.J., van den Tweel, J.G., de Weger, R.A., 2007. Type IV collagen degradation in the myocardial basement membrane after unloading of the failing heart by a left ventricular assist device. Lab. Invest. 87 (11), 1125–1137. https://doi.org/10.1038/labinvest.3700670.

Carpenter, A.E., Jones, T.R., Lamprecht, M.R., Clarke, C., Kang, I.H., Friman, O., Guertin, D.A., Chang, J.H., Lindquist, R.A., Moffat, J., Golland, P., Sabatini, D.M., 2006. Cell Profiler: image analysis software for identifying and quantifying cell phenotypes. Genome Biol. 7 (10) https://doi.org/10.1186/gb-2006-7-10-r100.

Chapman, D., Weber, K.T., Eghbali, M., 1990. Regulation of fibrillar collagen types I and III and basement membrane type IV collagen gene expression in pressure overloaded rat myocardium. Circ Res. 67 (4), 787–794. https://doi.org/10.1161/01.res.67.4.787. PMID: 2145089.

Frantz, S., Hu, K., Adamek, A., Wolf, J., Sallam, A., Maier, S.K.G., Lonning, S., Ling, H., Ertl, G., Bauersachs, J., 2008. Transforming growth factor beta inhibition increases mortality and left ventricular dilatation after myocardial infarction. Basic Res. Cardiol. 103 (5), 485–492. https://doi.org/10.1007/s00395-008-0739-7.

Hackett, T.L., Vriesde, N.R.T.F., Al-Fouadi, M., Mostaco-Guidolin, L., Maftoun, D., Hsieh, A., Coxson, N., Usman, K., Sin, D.D., Booth, S., Osei, E.T., 2022. The role of the dynamic lung extracellular matrix environment on fibroblast morphology and inflammation. Cells 11 (2). https://doi.org/10.3390/cells11020185.

Hammoud, L., Lu, X., Lei, M., 2011. Deficiency in TIMP-3 increases cardiac rupture and mortality post-myocardial infarction via EGFR signaling: beneficial effects of cetuximab. pp. 459–471. doi: 10.1007/s00395-010-0147-7.

Hou, X., Liu, S., Wang, M., Wiraja, C., Huang, W., Chan, P., Tan, T., Xu, C., 2017. Layer-by-layer 3D constructs of fibroblasts in hydrogel for examining transdermal penetration capability of nanoparticles. SLAS Technol. 22 (4), 447–453. https://doi.org/10.1177/2211068216655753.

Ichihara, S., Senbonmatsu, T., Price, E., Ichiki, T., Gaffney, F.A., Inagami, T., 2002. Targeted deletion of angiotensin II type 2 receptor caused cardiac rupture after acute myocardial infarction. Circulation 106 (17), 2244–2249. https://doi.org/10.1161/01.CIR.0000033826.52681.37.

Kural, M.H., Billiar, K.L., 2016. Myofibroblast persistence with real-time changes in boundary stiffness. Acta Biomater. 32, 223–230. https://doi.org/10.1016/j.actbio.2015.12.031.

Ma, Y., Halade, G.V., Zhang, J., Ramirez, T.A., Levin, D., Voorhees, A., Jin, Y.F., Han, H. C., Manicone, A.M., Lindsey, M.L., 2013. Matrix metalloproteinase-28 deletion exacerbates cardiac dysfunction and rupture after myocardial infarction in mice by inhibiting M2 macrophage activation. Circ. Res. 112 (4), 675–688. https://doi.org/10.1161/CIRCRESAHA.111.300502.

Miyazaki, K., Oyanagi, J., Hoshino, D., Togo, S., Kumagai, H., Miyagi, Y., 2019. Cancer cell migration on elongate protrusions of fibroblasts in collagen matrix. Sci. Rep. 9 (1) https://doi.org/10.1038/s41598-018-36646-z.

Parsa, H., Wang, B.Z., Vunjak-Novakovic, G., 2017. A microfluidic platform for the high-throughput study of pathological cardiac hypertrophy. Lab Chip 17 (19), 3264–3271. https://doi.org/10.1039/c7lc00415j.

Richardson, W.J., Clarke, S.A., Alexander Quinn, T., Holmes, J.W., 2015. Physiological implications of myocardial scar structure. Compr. Physiol. 5 (4), 1877–1909. https://doi.org/10.1002/cphy.c140067.

Richardson, W.J., Holmes, J.W., 2016. Emergence of collagen orientation heterogeneity in healing infarcts and an agent-based model. Biophys. J. 110 (10), 2266–2277. https://doi.org/10.1016/j.bpj.2016.04.014.

Richardson, W.J., Rogers, J.D., Spinale, F.G., 2021. Does the heart want what it wants? A case for self-adapting, mechano-sensitive therapies after infarction. Front. Cardiovasc. Med. 8, 705100 https://doi.org/10.3389/fcvm.2021.705100.

Rogers, J.D., Holmes, J.W., Saucerman, J.J., Richardson, W.J., 2021. Mechano-chemo signaling interactions modulate matrix production by cardiac fibroblasts. Matrix Biol. Plus 10, 100055. https://doi.org/10.1016/j.mbplus.2020.100055.

Schmidt, J.B., Chen, K., Tranquillo, R.T., 2016. Effects of intermittent and incremental cyclic stretch on ERK signaling and collagen production in engineered tissue. Cell. Mol. Bioeng. 9 (1), 55–64. https://doi.org/10.1007/s12195-015-0415-6.

Smithmyer, M.E., Sawicki, L.A., Kloxin, A.M., 2014. Hydrogel scaffolds as in vitro models to study fibroblast activation in wound healing and disease. In: Biomaterials Science, Vol. 2, Issue 5. Royal Society of Chemistry, pp. 634–650. doi: 10.1039/c3bm60319a.

Walker, M., Godin, M., Pelling, A.E., 2020a. Mechanical stretch sustains myofibroblast phenotype and function in microtissues through latent TGF-β1 activation. Integr. Biol. 12 (8), 199–210. https://doi.org/10.1093/intbio/zyaa015.

Walker, M., Godin, M., Harden, J.L., Pelling, A.E., 2020b. Time dependent stress relaxation and recovery in mechanically strained 3D microtissues. APL Bioeng. 4 (3) https://doi.org/10.1063/5.0002898.

Walker, M., Rizzuto, P., Godin, M., Pelling, A.E., 2020c. Structural and mechanical remodeling of the cytoskeleton maintains tensional homeostasis in 3D microtissues under acute dynamic stretch. Sci. Rep. 10 (1) https://doi.org/10.1038/s41598-020-64725-7.

Zhang, T., Day, J.H., Su, X., Guadarrama, A.G., Sandbo, N.K., Esnault, S., Denlinger, L.C., Berthier, E., Theberge, A.B., 2019. Investigating fibroblast-induced collagen gel contraction using a dynamic microscale platform. Front. Bioeng. Biotechnol. 7 (AUG) https://doi.org/10.3389/fbioe.2019.00196.